Research Article Vol. 9, No. 12 / December 2022 / Optica 1333

All-optical spin injection in silicon investigated by element-specific time-resolved Kerr effect

Simone Laterza,[1,2,*] Antonio Caretta,[1,7] Richa Bhardwaj,[1] Roberto Flammini,[3] Paolo Moras,[4] Matteo Jugovac,[4] Piu Rajak,[5] Mahabul Islam,[5] Regina Ciancio,[5] Valentina Bonanni,[1] Barbara Casarin,[2] Alberto Simoncig,[1] Marco Zangrando,[1,5] Primož Rebernik Ribič,[1] Giuseppe Penco,[1] Giovanni De Ninno,[1] Luca Giannessi,[1] Alexander Demidovich,[1] Miltcho Danailov,[1] Fulvio Parmigiani,[1,6] and Marco Malvestuto[1,5]

[1]Elettra Sincrotrone Trieste, S.C.p.A. Strada Statale 14-km 163.5 in AREA Science Park 34149 Basovizza, Trieste, Italy
[2]Department of Physics, University of Trieste, Via A. Valerio 2, 34127 Trieste, Italy
[3]Istituto di Struttura della Materia-CNR (ISM-CNR), Via del Fosso del Cavaliere 100, 00133, Roma, Italy
[4]Istituto di Struttura della Materia-CNR (ISM-CNR), SS 14 km 163.5, I-34149, Trieste, Italy
[5]Istituto Officina dei Materiali (CNR-IOM), SS 14 km 163.5, I-34149, Trieste, Italy
[6]International Faculty, University of Cologne, 50937 Cologne, Germany
[7]e-mail: antonio.caretta@elettra.eu
*Corresponding author: simone.laterza@elettra.eu

Received 28 July 2022; revised 19 September 2022; accepted 20 September 2022; published 28 November 2022

Understanding how a spin current flows across metal-semiconductor interfaces at pico- and femtosecond time scales is of paramount importance for ultrafast spintronics, data processing, and storage applications. However, the possibility to directly access the propagation of spin currents, within such time scales, has been hampered by the simultaneous lack of both ultrafast element-specific magnetic sensitive probes and tailored well-built and characterized metal-semiconductor interfaces. Here, by means of a novel free-electron laser-based element-sensitive ultrafast time-resolved Kerr spectroscopy, we reveal different magnetodynamics for the Ni $M_{2,3}$ and Si $L_{2,3}$ absorption edges. These results are assumed to be the experimental evidence of photoinduced spin currents propagating at a speed of ∼0.2 nm/fs across the Ni/Si interface.

https://doi.org/10.1364/OPTICA.471951

1. INTRODUCTION

Nowadays, spin-based electronics (spintronics) has been compared favorably to conventional electronics because of the lower switching energy and the higher switching speed [1,2]. The main reasons are that spin currents (SCs) are suggested to flow nearly dissipationless [3,4], while spin coherence time is larger than the charge confinement lifetime [5]. In particular, this applies to the injection of the superdiffusive SCs through some metal/metal interfaces [6,7].

SCs are generated inside ferromagnetic metals by means of ultrashort infrared (IR) pulses [8,9] where a spin-preserving out-of-equilibrium hot electron distribution is created [6]. Since in ferromagnetic metals the excited carriers lifetime and velocity are much larger for spin majority electrons, an ultrashort SC pulse is set. SCs have been reported in Ni/Au, Ni/Fe, Fe/Pt, and Ni/Co-Pt multilayers [10–13]. Besides, SCs in the form of propagating magnons triggered by ultrafast optical pulses have been observed for NiO [14], CoO [15], and ZnO [16]. Conversely, the spin injection into some technologically relevant semiconductors is still an open question. Silicon, by allowing long-lived SCs because of the small spin–orbit interaction, the reduced nuclear spin, and the crystal inversion symmetry, is a good candidate for these studies [4,17,18].

A recent theoretical work [8] proposes the spin injection from nickel to silicon to be chargeless, i.e., independent from the charge carrier flow, up to 80% spin-polarized, and ultrashort.

However, an experimental benchmark about the spin injection at the ferromagnet/silicon interface, such as the measures of the magnitude of spin accumulation, the spin lifetimes, and the SC velocity, is lacking [19,20]. To provide this information is also challenging because an effective control of the potential barrier at the metal/semiconductor interface must be achieved; hence, its effective manufacturing and structural characterization are of critical importance.

Here, we report about a novel ultrafast time-resolved resonant magneto-optical Kerr effect experiment (TR-RMOKE) [21,22] at Si $L_{2,3}$ and Ni $M_{2,3}$ absorption edges. Thanks to the element selectivity of the TR-RMOKE spectroscopy, performed at an externally seeded and tunable free-electron laser (FEL) and to a state-of-the-art fabrication and characterization of the Ni/Si interface, we can decouple the magnetodynamical response of the Si support from the Ni overlayer. In particular, the slower demagnetization

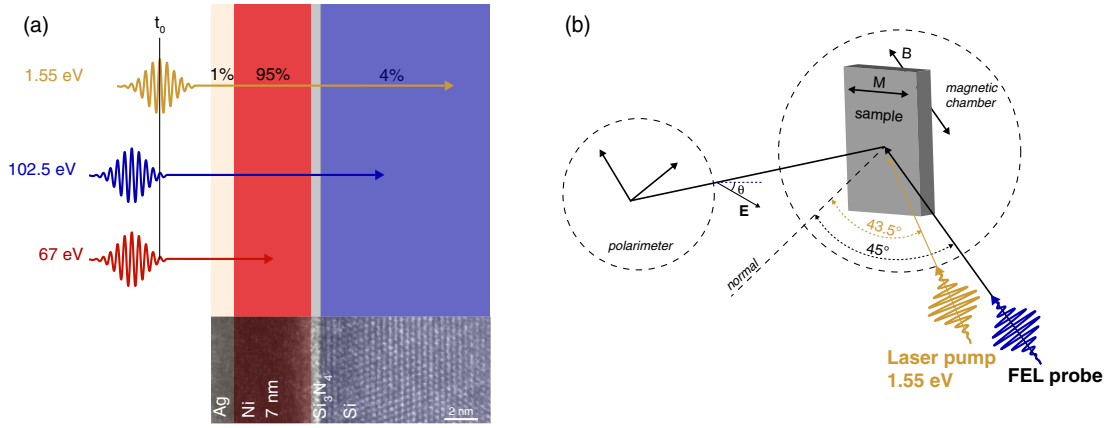

Fig. 1. (a) Schematic representation of the sample stack consisting of a Si substrate (blue), a thin Si_3N_4 passivation layer (gray), 7 nm of Ni film (red), and 2 nm of Ag capping layer (yellow). At time t_0, the IR laser pulses (1.55 eV, gold arrow) hit the sample. The FEL pulses, tuned at the Si $L_{2,3}$ edge (102.5 eV, blue arrow) and at the Ni $M_{2,3}$ edge (67 eV, red arrow), probe the sample status at later time scales. The penetration depth of the pump and of the probe pulses is represented by the length of the respective arrows. The fraction (as percentage) of the total energy of the IR laser absorbed by each layer is reported above the pump arrow. An HRTEM image of the heterostructure is superimposed to the lower part of the schematic. (b) Scheme of the FEL RMOKE setup at MagneDyn. The pump and probe pulses are in a quasi-collinear configuration. RMOKE was probed in longitudinal configuration at an angle of incidence of 45°. The linear polarization E of the FEL pulses reflected from the sample is rotated with respect to the scattering plane (dashed line) of the Kerr angle θ.

response detected at the Si edge is interpreted as an evidence of a transient SC, propagating at ∼0.2 nm/s [8], from Ni into Si.

2. EXPERIMENT

We investigated the Ag/Ni/$\beta-Si_3N_4$ (0001)/Si(111) interface (from now on called Ni/Si for short) whose structure is schematically represented in Fig. 1(a). The sample was synthesized at the VUV-Photoemission beamline (Elettra Sincrotrone Trieste) according to the recipe of [23,24]. Section I of Supplement 1 reports on the X-ray photoelectron spectroscopy (XPS) characterization of the sample. The substrate used for the deposition was a p-doped (B dopant, $0.05\Omega \cdot$cm resistivity) Si(111) -7×7 surface reconstructed substrate. Nitride passivation of the Si surface was required in order to reduce the formation of unwanted metallic silicides and diminish the migration of the metallic ions into the substrate. Subsequently, 7 nm of Ni was deposited at a low temperature to form epitaxial layers [25]. A silver capping layer of 2 nm was grown to avoid the oxidation of the Ni layer. After the experiment, the interface was characterized by high resolution transmission electron microscopy (HRTEM), as shown in Fig. 1(a). The observation of a sharp Ni/Si interface confirms that both the formation of silicides and the pump beam damage were under control. Thanks to HRTEM, we estimate the thickness of the Si_3N_4 layer to be ∼0.7 nm. Moreover, no Ni oxide formation was detected. Further details on HRTEM measurements are provided in Section II of Supplement 1.

The room-temperature transient magnetic response of our sample was measured via the longitudinal RMOKE in a pump-probe scheme, which allows one to detect the effects on the sample magnetization **M** induced by an IR pump beam. All the RMOKE measurements were carried out at the MagneDyn end-station [26] at the externally seeded EUV FEL FERMI [27] at Elettra Sincrotrone Trieste.

A schematic illustration of the experimental scattering configuration is shown in Fig. 1(b). The sample was excited by a ∼70 fs pump pulse at 1.55 eV with a 25 Hz repetition rate decimated with respect to the FEL 50 Hz repetition rate for achieving the standard pump-on/off data acquisition mode. The IR pump pulse was generated from the same laser used to seed the FERMI FEL and had a root mean square timing jitter with respect to the FEL pulses of ∼7 fs [28]. The angle of incidence of the incoming IR pump pulse is 43.5°. The probe consists of ∼50 fs FEL light pulses whose energy is tuned to the absorption edges of Ni and Si. The electric field of the linearly polarized incoming light lays in the scattering plane, while the angle of incidence was set to 45°. The fluences of the IR pump pulses at the sample were 60 mJ/cm^2 for the measurements at the Ni $M_{2,3}$ edge and 15 mJ/cm^2 for the Si $L_{2,3}$ edge. Instead, the FEL fluences were 4.0 mJ/cm^2 at the Ni $M_{2,3}$ edge and 1.2 mJ/cm^2 at the Si $L_{2,3}$ edge, respectively. Please note that the fluence is considered at $1/e^2$ as in [29]. Considering the reflectivity and absorbance coefficients of the overall sample stack at 1.55 eV [30] and limiting the absorption up to the first 100 nm of the Si substrate, the fraction of the total absorbed intensity of the incoming optical pump pulse released in the Ni layer is 95%. The remaining energy is absorbed by the Ag capping layer (1%) and the Si substrate (4%).

The RMOKE analysis of the FEL light polarization angle θ as a function of the pump-probe time delay $(t-t_0)$ is carried out with a Wollaston-like polarimeter that collects the reflected FEL pulses [31]. The polarimeter decomposes the polarization of the beam in two orthogonal components with I_1 and I_2 intensities. The polarization angle of the reflected beam with respect to the scattering plane is then approximated as [32]

$$\theta = \frac{1}{2}\frac{I_1 - I_2}{I_1 + I_2}. \quad (1)$$

Element sensitivity to Ni and Si is achieved by resonantly tuning the FEL radiation at the Ni $M_{2,3}$ edge [33] and the Si $L_{2,3}$ edge [34], which are 35 eV apart. This energy separation guarantees that the resonant response of the magneto-optical tensors of the two elements do not overlap. A confirmation to this comes also from *ab initio* calculation of the Ni Kerr rotation away from the Ni $M_{2,3}$ edge in the energy region of the Si $L_{2,3}$ edge. Details of

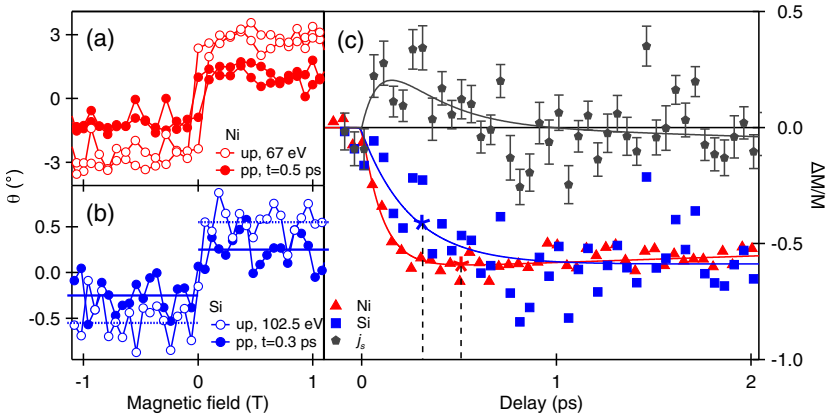

Fig. 2. RMOKE magnetic hysteresis in degrees of Kerr rotation (a) at the Ni $M_{2,3}$ edge and (b) at the Si $L_{2,3}$ edge. The empty and filled circle curves represent the unpumped (labeled up) and pumped (labeled pp) hysteresis measured at a delay time of 0.5 ps (for the Ni edge) and 0.3 ps (for the Si edge), as indicated by the corresponding star marks in (c). (c) Relative change of the site resolved magnetization M as a function of the time delay measured in saturation with an applied magnetic field of 550 mT (Ni and Si, red and blue dots, respectively). The Ni demagnetization curve was rescaled to account for the different pump fluences applied. The solid lines represent the best fit to the data, from which we extracted the two characteristic times for demagnetization (τ_m) and recovery (τ_r). The difference between the two magnetization dynamics, defined as $(\Delta\mathbf{M}/\mathbf{M})_{j_s}$, is also shown (gray pentagons). The gray curve is a guide to the eye for $(\Delta\mathbf{M}/\mathbf{M})_{j_s}$.

the calculation are reported in the Supplement 1, Section III. The applied magnetic field **B**, whose direction is parallel to the *k*-vector of the incoming FEL radiation, orients the magnetization of Ni along the line of intersection between the sample surface and the plane of incidence.

Finally, the transient relative change of the sample magnetization magnitude **M** is defined as

$$\frac{\Delta\mathbf{M}}{\mathbf{M}}(t) = \frac{\theta(t)^+ - \theta(t)^-}{\theta_{\text{sat}}^+ - \theta_{\text{sat}}^-}, \tag{2}$$

where t is the delay time between the probe and the pump arrival, $\theta(t)^\pm$ represents the RMOKE signals, and $\theta_{\text{sat}}^\pm$ represents the RMOKE unpumped saturation values at opposite magnetic fields.

3. RESULTS

Figure 2(a) displays the Kerr rotation collected at the Ni $M_{2,3}$ edge (67 eV) as a function of the applied magnetic field taken before the pump arrival (empty circles) and 500 fs after the pump absorption (filled circles). The Si Kerr rotation collected with the FEL photon energy resonantly tuned to the Si $L_{2,3}$ edge (102.5 eV) and taken before and at a 300 fs time delay after the pump arrival is reported in Fig. 2(b). The Kerr rotation displays a hysteresis shape for both the Ni and the Si edges. The measured coercitivity field for Ni is ∼50 mT, which confirms the ferromagnetic state of the Ni layer. We notice that the observation of a finite Kerr magnetic signal at the Si edge for negative time delays is not expected because Si is a weakly diamagnetic material. Some possible mechanisms that would allow this kind of effect will be given in the Section 4. Please note that it is not possible to make an absolute comparison between $\theta_{\text{sat}}^\pm$Ni and $\theta_{\text{sat}}^\pm$Si since the Kerr rotation depends on several factors as the magneto-optical constant, the experimental geometry, the layer stack structure, and eventually the magnetization of each element. Anyways, Figs. 2(a) and 2(b) show that the pump arrival causes a decrease of the amplitude of the Kerr hysteresis, expressed by $\theta_{\text{sat}}^+ - \theta_{\text{sat}}^-$, for both the Ni and the Si edges. This is consistent with a reduction of the magnetization in both layers.

Table 1. Demagnetization (τ_m) and Recovery (τ_r) Time Values Extracted from the Fitting to the Data of Fig. 2(c)[a]

	τ_m (fs)	τ_r (ps)
Ni	**100 ± 12**	**20.3 ± 5.6**
	140 ± 10 [7]	—
	208 ± 33 [10]	22 ± 17 [10]
Si	**255 ± 86**	**> 100**

[a]In bold, our results compared to the values present in the literature.

Figure 2(c) displays the characteristic dynamics of the ultrafast relative change of the layer magnetization $\Delta M/M$ measured at fixed FEL photon energies resonantly tuned to the Ni (red marks) and the Si (blue marks) edges with a saturating external field of 550 mT. The relative difference between the two dynamics is also reported (gray pentagons). In order to retrieve the characteristic lifetimes of the ultrafast magnetodynamics, the demagnetization curves were fitted using a decay-recovery double-exponential function,

$$f(t) = \frac{\Delta\mathbf{M}}{\mathbf{M}}\Theta(t)(1 - e^{-t/\tau_m})e^{-t/\tau_r}, \tag{3}$$

where $\Theta(t)$ is the Heaviside step function, and τ_m and τ_r are the demagnetization and the recovery times, respectively. Results of the fitting are shown in Fig. 2(c) and summarized in Table 1 together with typical demagnetization and recovery times of Ni found in earlier experiments [7,10].

4. DISCUSSION

Figure 3 summarizes our experimental findings and outlines the possible magnetic configuration of the interface. The initial state consists of a magnetized Ni film and a magnetized Si substrate, as revealed by the measured RMOKE hysteresis in Figs. 2(a) and 2(b). Unlike the Ni film case, the origin of the static magnetized state of the Si substrate is not trivial, and some alternative hypotheses are here considered.

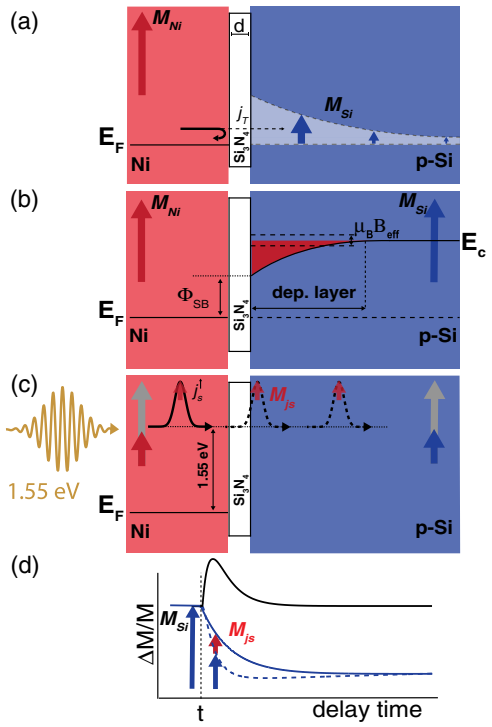

Fig. 3. Display of (a), (b) shows the proximity effect in the Ni/Si interface, and (c), (d) shows the accompanying magnetic dynamics in both the Ni film (red, $\mathbf{M}_{\mathrm{Ni}}$) and the Si substrate (blue, $\mathbf{M}_{\mathrm{Si}}$). (a) Thermal electrons that impinge the Schottky barrier are spin-polarized; by tunneling the thin Si_3N_4 layer ($d = 0.7$ nm), they generate a spin-polarized current (j_T, black solid and dashed arrows). (b) Energy band diagram of the Ni/Si interface, with a focus on the depletion layer populated by spin-polarized electrons (red area). (c) Right after the arrival of the pump pulse (golden wave), the magnetization of the Ni layer is quenched. This triggers a demagnetization of the Si and simultaneously the injection of a superdiffusive SC (j_s, black pulse) into Si, carrying a magnetic moment $\mathbf{M}_{\mathrm{js}}$ (small red arrows). (d) The two phenomena compete and cause the slow down of the demagnetization rate in Si (blue arrows and dashed curve).

The injection of spins from metals into semiconductors is a complex topic, subject of intense investigations over the last 20 years. Initially, researchers focused on the so-called conductivity mismatch problem [35]. This obstacle refers to the large conductivity difference between the metal and the semiconductor that limits the spin polarization below 0.1%. Soon later, it was showed that, with a tunnel barrier separating the metal and the semiconductor, an efficient spin injection was possible [36,37]. Since then, several experimental groups had successfully measured the spin injection. The vast majority of these studies investigate the spin polarization with an external applied electric field bias [38–40]. The results of these studies cannot be directly applied to our investigation, where there is no external electric field. In fact, as far as we understand, the magnetization of the semiconductor without a bias cannot be calculated starting from the same equations used for the transport. For instance, in [36], the spin up J^+ and the spin down J^- currents are proportional to the applied bias and, thus, are zero at zero field. Yet, zero-polarized current does not imply that there is no static spin polarization in silicon. Unfortunately, very few articles focus on the spin-polarized electron density. We are aware of two experiments measuring a net spin polarization of the semiconductor at zero bias. The first [41] claims that there is an effective long-range $p-d$ exchange between the Co and (Cd,Mg)Te layer. This effect might occur as well at the Ni/Si interface, through the d orbitals of Ni and the p orbitals of Si. A second experimental observation concerns the ferromagnetic-proximity polarization (FPP) [42,43], where the nuclear spin polarization in the semiconductor plays a fundamental role. Unfortunately, these two models are not supported by an established theoretical framework readily applicable to our case. Accordingly, here we are using the simplest models that can explain the spin polarization of the silicon layer.

We identified two possible models that can explain the origin of the magnetism in silicon, both relying on the proximity effect of the Si substrate to the magnetized Ni layer.

The first model [Fig. 3(a)] relies on the presence of low-energy thermal electrons in Ni. As they diffuse at equilibrium in the metallic layer, spin minority and majority electrons experience a different exchange interaction with the mainly spin-majority-polarized electron background. Accordingly, spin minority electrons are more scattered with respect to spin majority ones, resulting in shorter lifetimes and velocities with respect to their spin majority counterparts. As a result, thermal electrons that impinge the Ni/Si interface are also spin-polarized, and they can diffuse as a tunneling current [j_T, solid black arrow in Fig. 3(a)] inside the Si substrate [40]. Only a fraction of the electrons impinging the interface are injected into the semiconductor (dashed black arrow). Because there is no net charge current without an external bias, this charge flux from Ni to Si must be balanced at equilibrium by a current flowing in the opposite direction. However, the spin polarization of the two currents can be different, resulting in a net spin accumulation in the proximal layer of Si (shaded white profile) [40].

A second possible origin to the magnetization in Si [Fig. 3(b)] is due to the proximity magnetic field that causes the electrons in the conduction band to be spin-polarized in the depletion layer. Please note that, while our system is technically a metal/insulator/semiconductor interface, it behaves as a sharp metal/silicon interface, due to the thinness of the insulator interlayer. In fact, the interface forms a Schottky barrier varying linearly with the thickness, with no pinning of the Fermi level [44]. The energy band diagram of the Ni/Si Schottky interface has been shown in Fig. 3(b); the B doping level of 9.3×10^{17} cm^{-3} gives rise to an estimated Schottky barrier height Φ_{SB} of $+0.02$ eV [44] and a depletion layer of $\sim$40 nm. Due to the presence of the magnetized metal, the electrons in Si will perceive an effective magnetic field causing an exchange splitting $\Delta E_{\mathrm{ex}} = \mu_B \cdot B_{\mathrm{eff}}$—where μ_B is the Bohr magneton and B_{eff} is the effective magnetic field—determining a net spin majority polarization localized in the depletion layer region. Accordingly, any change of the magnetization in Ni will affect almost instantaneously the effective field —$\Gamma/c = 55$ nm/c ~ 0.2 fs—where Γ is the attenuation length at the Si $L_{2,3}$ edge—and, therefore, the spin unbalance of electrons in Si, resulting in a fast electron coupling between the Ni and Si spin-polarized electron populations.

Besides this, we underline that HRTEM analysis identified only small traces of silicide formation (Supplement 1), in particular of $NiSi_2$, between the silicon substrate and the nitride layer. Yet, because $NiSi_2$ is expected to be nonmagnetic from the literature [45,46], we can discard the contribution of this effect to the static magnetization of Si.

Although the two models described above qualitatively explain the magnetization of the Si substrate before the pump arrival, further investigations are ongoing to elucidate this point.

In Fig. 3(c), the magnetodynamics at the Ni and Si edges is displayed. The optical absorption of an ultrafast pulse by the Ni film is accompanied by a sudden increase of the electron temperature and a consequent reduction of the spin polarization of the exchange-split Ni bands. In turn, while the Ni film demagnetizes in ∼100 fs, the consequent reduction of the spin polarization of the Ni bands reflects in a reduction of the spin polarization of the electrons in Si. Accordingly, $\mathbf{M}_{\mathrm{Si}}$ diminishes as revealed by the magnetodynamics at the Si edge. The most striking feature of Fig. 2(c) is that within the first ∼1 ps the Ni and Si ($\Delta\mathbf{M}/\mathbf{M}$) exhibit different dynamical responses to the laser excitation.

Specifically, $\mathbf{M}_{\mathrm{Si}}$ reacts 2.5 times slower than $\mathbf{M}_{\mathrm{Ni}}$, as can be seen in Fig. 2(c) from the resulting demagnetization rates of change in the two materials. The difference $(\Delta\mathbf{M}/\mathbf{M})_{\mathrm{Si}} - (\Delta\mathbf{fM}/\mathbf{M})_{\mathrm{Ni}}$, which is indicated as $(\Delta\mathbf{M}/\mathbf{M})_{j_s}$, is plotted in Fig. 2(c) (gray pentagons), and it represents the transient SC j_s. The propagation of j_s is illustrated in Fig. 3(c). In the absence of any SC injection, we expect the dynamics at the two edges to be the same, as a consequence of the presence of the proximity effect. As displayed in Fig. 3(d), the propagation of j_s competes instead with the demagnetization of the Si substrate, resulting in a longer demagnetization time τ_m in Si. Consequently, based on this scenario, we can consider the difference between the Ni $M_{2,3}$ and Si $L_{2,3}$ magnetodynamics $(\Delta\,\mathbf{M}/\mathbf{M})_{j_s}$ as an experimental evidence of the onset and propagation of a superdiffusive SC across the Ni/Si interface. On a longer time scale, following the propagation of the SC pulse inside the Si substrate, the observed j_s contribution becomes irrelevant. Finally, having established the presence of a SC injected in the Si substrate across a Ni/Si interface, further quantitative information could also be extracted. $(\Delta\,\mathbf{M}/\mathbf{M})_{j_s}$ displays a maximum at ∼150 fs after the pump arrival, followed by an exponential decay time $\tau = 248 \pm 128$ fs, as obtained by an exponential fitting of the trace [see also the gray guide for the eye in Fig. 2(c)]. Considering the SC pulse decay time as $\tau = \Gamma/v$, the calculated velocity v of the spin pulse propagating in the Si substrate results to be $\Gamma/\tau \sim 0.2$ nm/fs. This experimental finding matches the theoretical predictions made on an ideal Ni/Si system [8].

5. CONCLUSION

In summary, we used element-specific time-resolved magneto-optical Kerr effect spectroscopy (TR-MOKE) at the Ni $M_{2,3}$ and Si $L_{2,3}$ edges in a Ni/Si interface at the externally seeded FERMI FEL. Contrary to expectation, the Si substrate is observed to be already magnetized before the pump arrival. We presented two possible models that can be the origin of the magnetization of Si, either in terms of tunneling of spin-polarized electrons from the Ni magnetic layer or in terms of modification of the exchange splitting of the electrons in the silicon depletion layer induced by the effective magnetic field. Both effects can qualitatively explain the observed magnetization of Si and can even occur simultaneously. Upon the pump arrival, the demagnetization of Si competes with the onset and propagation of the transient SC from Ni, slowing down the demagnetization lifetime in Si. Our experimental findings now call for further theoretical investigations aiming at modeling the equilibrium and non-equilibrium dynamics at the magnetic metal/silicon interfaces.

Funding. EUROFEL–ROADMAP ESFRI.

Acknowledgment. A. C. and F. P. would like to thank Marco Battiato for fruitful discussion. P. M. and M. J. acknowledge financial funding though the project EUROFEL–ROADMAP ESFRI.

Disclosures. The authors declare no conflicts of interest.

Data availability. Data underlying the results presented in this paper are not publicly available at this time but may be obtained from the authors upon reasonable request.

Supplemental document. See Supplement 1 for supporting content.

REFERENCES

1. D. D. Awschalom and M. E. Flatté, "Challenges for semiconductor spintronics," Nat. Phys. **3**, 153–159 (2007).
2. K. L. Wang, J. G. Alzate, and P. K. Amiri, "Low-power non-volatile spintronic memory: STT-RAM and beyond," J. Phys. D **46**, 074003 (2013).
3. S. Murakami, N. Nagaosa, and S.-C. Zhang, "Dissipationless quantum spin current at room temperature," Science **301**, 1348–1351 (2003).
4. I. Žutić, J. Fabian, and S. D. Sarma, "Spintronics: fundamentals and applications," Rev. Mod. Phys. **76**, 323–410 (2004).
5. B. Huang, D. J. Monsma, and I. Appelbaum, "Coherent spin transport through a 350 micron thick silicon wafer," Phys. Rev. Lett. **99**, 177209 (2007).
6. M. Battiato, K. Carva, and P. M. Oppeneer, "Superdiffusive spin transport as a mechanism of ultrafast demagnetization," Phys. Rev. Lett. **105**, 027203 (2010).
7. A. Eschenlohr, M. Battiato, P. Maldonado, N. Pontius, T. Kachel, K. Holldack, R. Mitzner, A. Föhlisch, P. M. Oppeneer, and C. Stamm, "Ultrafast spin transport as key to femtosecond demagnetization," Nat. Mater. **12**, 332–336 (2013).
8. M. Battiato and K. Held, "Ultrafast and gigantic spin injection in semiconductors," Phys. Rev. Lett. **116**, 196601 (2016).
9. M. Battiato, "Spin polarisation of ultrashort spin current pulses injected in semiconductors," J. Phys. Condens. Matter **29**, 174001 (2017).
10. D. Rudolf, C. La-O-Vorakiat, M. Battiato, R. Adam, J. M. Shaw, E. Turgut, P. Maldonado, S. Mathias, P. Grychtol, H. T. Nembach, T. J. Silva, M. Aeschlimann, H. C. Kapteyn, M. M. Murnane, C. M. Schneider, and P. M. Oppeneer, "Ultrafast magnetization enhancement in metallic multilayers driven by superdiffusive spin current," Nat. Commun. **3**, 1037 (2012).
11. T. Kampfrath, M. Battiato, P. Maldonado, G. Eilers, J. Nötzold, S. Mährlein, V. Zbarsky, F. Freimuth, Y. Mokrousov, S. Blügel, M. Wolf, I. Radu, P. M. Oppeneer, and M. Münzenberg, "Terahertz spin current pulses controlled by magnetic heterostructures," Nat. Nanotechnol. **8**, 256–260 (2013).
12. X.-P. He, P.-H. Huang, X.-Y. Yang, Z.-M. Jin, S.-T. Lou, X.-L. Zhang, and Q.-Y. Jin, "Comparative study of coherent terahertz emission from Fe/Pt ferromagnetic heterostructures," Chin. Opt. Lett. **17**, 081601 (2019).
13. T. Seifert, S. Jaiswal, U. Martens, *et al.*, "Efficient metallic spintronic emitters of ultrabroadband terahertz radiation," Nat. Photonics **10**, 483–488 (2016).
14. K. Lee, D.-K. Lee, D. Yang, R. Mishra, D.-J. Kim, S. Liu, Q. Xiong, S. K. Kim, K.-J. Lee, and H. Yang, "Superluminal-like magnon propagation in antiferromagnetic NiO at nanoscale distances," Nat. Nanotechnol. **16**, 1337–1341 (2021).
15. Y. Sasaki, G. Li, T. Moriyama, T. Ono, R. V. Mikhaylovskiy, A. V. Kimel, and S. Mizukami, "Laser stimulated THz emission from Pt/CoO/FeCoB," Appl. Phys. Lett. **117**, 192403 (2020).
16. M. Althammer, E.-M. Karrer-Müller, S. T. B. Goennenwein, M. Opel, and R. Gross, "Spin transport and spin dephasing in zinc oxide," Appl. Phys. Lett. **101**, 082404 (2012).
17. A. M. Tyryshkin, S. A. Lyon, A. V. Astashkin, and A. M. Raitsimring, "Electron spin relaxation times of phosphorus donors in silicon," Phys. Rev. B **68**, 193207 (2003).
18. I. Žutić and H. Dery, "Taming spin currents," Nat. Mater. **10**, 647–648 (2011).
19. V. Sverdlov and S. Selberherr, "Silicon spintronics: progress and challenges," Phys. Rep. **585**, 1–40 (2015).
20. R. Jansen, "Silicon spintronics," Nat. Mater. **11**, 400–408 (2012).
21. S. Yamamoto and I. Matsuda, "Measurement of the resonant magneto-optical Kerr effect using a free electron laser," Appl. Sci. **7**, 662 (2017).
22. X. Liu, A. Merhe, E. Jal, R. Delaunay, R. Jarrier, V. Chardonnet, M. Hennes, S. G. Chiuzbaian, K. Légaré, M. Hennecke, I. Radu, C. V. K.

Schmising, S. Grunewald, M. Kuhlmann, J. Lüning, and B. Vodungbo, "Sub-15-fs x-ray pump and x-ray probe experiment for the study of ultrafast magnetization dynamics in ferromagnetic alloys," Opt. Express **29**, 32388–32403 (2021).
23. H. Ahn, C.-L. Wu, S. Gwo, C. M. Wei, and Y. C. Chou, "Structure determination of the Si_3N_4/Si(111)- (8 × 8) surface: a combined study of Kikuchi electron holography, scanning tunneling microscopy, and ab initio calculations," Phys. Rev. Lett. **86**, 2818–2821 (2001).
24. R. Flammini, P. Allegrini, F. Wiame, R. Belkhou, F. Ronci, S. Colonna, D. M. Trucchi, F. Filippone, S. K. Mahatha, P. M. Sheverdyaeva, and P. Moras, "Nearly-free electronlike surface resonance of a β–Si_3N_4(0001)/Si(111)–8 × 8 interface," Phys. Rev. B **91**, 075303 (2015).
25. R. Flammini, S. Colonna, P. M. Sheverdyaeva, M. Papagno, A. K. Kundu, and P. Moras, "Effect of a subnanometer thin insulator layer at the Ag/Si(111) interface through the observation of quantum well states," Phys. Rev. Mater. **5**, 084604 (2021).
26. C. Svetina, N. Mahne, L. Raimondi, A. Caretta, B. Casarin, M. Dell'Angela, M. Malvestuto, F. Parmigiani, and M. Zangrando, "MagneDyn: the beamline for magneto dynamics studies at FERMI," J. Synchrotron Radiat. **23**, 98–105 (2016).
27. E. Allaria, D. Castronovo, P. Cinquegrana, *et al.*, "Two-stage seeded soft-X-ray free-electron laser," Nat. Photon. **7**, 913–918 (2013).
28. M. B. Danailov, F. Bencivenga, F. Capotondi, F. Casolari, P. Cinquegrana, A. Demidovich, E. Giangrisostomi, M. P. Kiskinova, G. Kurdi, M. Manfredda, C. Masciovecchio, R. Mincigrucci, I. P. Nikolov, E. Pedersoli, E. Principi, and P. Sigalotti, "Towards jitter-free pump-probe measurements at seeded free electron laser facilities," Opt. Express **22**, 12869–12879 (2014).
29. Y. Liu, M. M. Aziz, A. Shalini, C. D. Wright, and R. J. Hicken, "Crystallization of $Ge_2Sb_2Te_5$ films by amplified femtosecond optical pulses," J. Appl. Phys. **112**, 123526 (2012).
30. M. Polyanskiy, "Refractive index database," 2021, http://refractiveindex.info.
31. A. Caretta, S. Laterza, V. Bonanni, R. Sergo, C. Dri, G. Cautero, F. Galassi, M. Zamolo, A. Simoncig, M. Zangrando, A. Gessini, S. D. Zilio, R. Flammini, P. Moras, A. Demidovich, M. Danailov, F. Parmigiani, and M. Malvestuto, "A novel free-electron laser single-pulse Wollaston polarimeter for magneto-dynamical studies," Struct. Dyn. **8**, 034304 (2021).
32. M. C. Donker, "Ultrafast optically-induced magnetization and conductivity dynamics in the europium chalcogenides," Ph.D. thesis (University of Groningen, 2014), Chap. 5, pp. 144, Eq. (5.17).
33. T. Koide, T. Shidara, H. Fukutani, K. Yamaguchi, A. Fujimori, and S. Kimura, "Strong magnetic circular dichroism at the M2,3 edges in ferromagnetic Ni and ferrimagnetic Fe_3O_4," Phys. Rev. B **44**, 4697–4700 (1991).
34. C. Antoniak, H. C. Herper, Y. N. Zhang, A. Warland, T. Kachel, F. Stromberg, B. Krumme, C. Weis, K. Fauth, W. Keune, P. Entel, R. Q. Wu, J. Lindner, and H. Wende, "Induced magnetism on silicon in Fe_3Si quasi-Heusler compound," Phys. Rev. B **85**, 214432 (2012).
35. G. Schmidt, D. Ferrand, L. W. Molenkamp, A. T. Filip, and B. J. van Wees, "Fundamental obstacle for electrical spin injection from a ferromagnetic metal into a diffusive semiconductor," Phys. Rev. B **62**, R4790–R4793 (2000).
36. A. Fert and H. Jaffrès, "Conditions for efficient spin injection from a ferromagnetic metal into a semiconductor," Phys. Rev. B **64**, 184420 (2001).
37. E. I. Rashba, "Theory of electrical spin injection: tunnel contacts as a solution of the conductivity mismatch problem," Phys. Rev. B **62**, R16267–16270 (2000).
38. E. I. Rashba, "Restrictions on modeling spin injection by resistor networks," Semicond. Sci. Technol. **23**, 114015 (2008).
39. S. P. Dash, S. Sharma, R. S. Patel, M. P. de Jong, and R. Jansen, "Electrical creation of spin polarization in silicon at room temperature," Nature **462**, 491–494 (2009).
40. A. Dankert, R. S. Dulal, and S. P. Dash, "Efficient spin injection into silicon and the role of the Schottky barrier," Sci. Rep. **3**, 3196 (2013).
41. V. L. Korenev, M. Salewski, I. A. Akimov, V. F. Sapega, L. Langer, I. V. Kalitukha, J. Debus, R. I. Dzhioev, D. R. Yakovlev, D. Müller, C. Schröder, H. Hövel, G. Karczewski, M. Wiater, T. Wojtowicz, Y. G. Kusrayev, and M. Bayer, "Long-range *p–d* exchange interaction in a ferromagnet-semiconductor hybrid structure," Nat. Phys. **12**, 85–91 (2016).
42. R. K. Kawakami, Y. Kato, M. Hanson, I. Malajovich, J. M. Stephens, E. Johnston-Halperin, G. Salis, A. C. Gossard, and D. D. Awschalom, "Ferromagnetic imprinting of nuclear spins in semiconductors," Science **294**, 131–134 (2001).
43. R. J. Epstein, I. Malajovich, R. K. Kawakami, Y. Chye, M. Hanson, P. M. Petroff, A. C. Gossard, and D. D. Awschalom, "Spontaneous spin coherence in N-GaAs produced by ferromagnetic proximity polarization," Phys. Rev. B **65**, 121202 (2002).
44. M. A. Sobolewski and C. R. Helms, "Properties of ultrathin thermal nitrides in silicon Schottky barrier structures," Appl. Phys. Lett. **54**, 638–640 (1989).
45. A. Dahal, J. Gunasekera, L. Harringer, D. K. Singh, and D. J. Singh, "Metallic nickel silicides: experiments and theory for NiSi and first principles calculations for other phases," J. Alloys Compd. **672**, 110–116 (2016).
46. L. Ma, J. Zhao, J. Wang, B. Wang, and G. Wang, "Magnetic properties of transition-metal impurities in silicon quantum dots," Phys. Rev. B **75**, 045312 (2007).